Structure of the deep lithosphere between Pamir and Tarim

Wasja Bloch[1], Bernd Schurr[1], Xiaohui Yuan[1], Lothar Ratschbacher[2], Sanaa Reuter[2], Sofia-Katerina Kufner[1,3], Qiang Xu[4,5], Junmeng Zhao[4,5]

[1]GFZ German Research Centre for Geosciences, 14473 Potsdam, Germany
[2]Geologie, Technische Universität Bergakademie Freiberg, 09599 Freiberg, Germany
[3]British Antarctic Survey, Cambridge CB3 0ET, England
[4]Key Laboratory of Continental Collision and Plateau Uplift, Institute of Tibetan Plateau Research, Chinese Academy of Sciences, Beijing 100101, China
[5]CAS Center for Excellence in Tibetan Plateau Earth Sciences, Beijing 100101, China

This manuscript is a non-peer reviewed preprint submitted to EarthArXiv. Submitted to *Geophysical Research Letters* (Wiley)

Key Points:

- Description of the overturned eastern end of the Asian slab and Kunlun intermediate depth seismicity
- Inference of the shape of the northern and eastern end of the Indian mantle indenter beneath the Pamir
- Publication of a new local earthquake catalog and seismic velocity model of the region

Corresponding author: Wasja Bloch, `wasja@gfz-potsdam.de`

Abstract

The Pamir orogen protrudes ∼300-km between the Tajik and Tarim lithosphere of central Asia. It is debated, whether its salient location and shape is controlled by indentation of a promontory of Indian mantle lithosphere or by rollback of thinned Tarim–Tajik-basin lithosphere. We present a new local-seismicity and focal-mechanism catalog and a P-wave velocity model of the previously poorly illuminated eastern Pamir and western Tarim lithosphere. The Wadati-Benioff earthquake zone that marks the arc-shaped Asian slab appears overturned in the eastern Pamir. In front of the Asian slab, another zone of weak earthquakes contours the western Kunlun, now accurately located to be interpreted in a local context. The seismic velocity structure guides our interpretation of this zone as a slice of eclogitizing Pamir plateau crust that lines a compressive transform zone boundary between a sub-crustal indenter and the Tarim block and favours an indentation- over a rollback-scenario.

Plain Language Summary

The Pamir highlands stand out distinctively between the Tajik basin to the west and the Tarim basin to the east. It is debated, whether the location and shape of this plateau is either caused by a part of the Indian continent that protrudes below Pamirs crust, or whether a thinned basin existed where the Pamir is now that made way during the collision of India with Asia. We present new seismological data that show that the Asian slab, that is a displaced part or slice of the Tarim–Tajik-basin, is overturned beneath the eastern Pamir. Additionally, we find a zone of high seismic velocities, indicative of a relatively cold and rigid structure, in front of the Asian slab. A seismically active zone of low seismic velocities is squeezed between this structure and the Tarim block. Together, these observations are clearly tracing the north and eastern margin of a mantle indenter that predefines the shape of the Pamir plateau.

1 Introduction

The salient Pamir plateau is part of the India-Asia collision system. It is distinctively offset to the North from the adjacent Tibet plateau by about 300 km and protrudes between the Tajik basin in the west and the cratonic block of the Tarim basin in the east (e.g. Lu et al., 2008). The northern Pamir and the Kunlun of northwestern Tibet comprise subduction-accretion-arc complexes accreted to and built on Asian continental basement. The central and southern Pamir and the Karakorum and Hindu-Kush represent Gondwana-derived microcontinents and subduction-accretion-arc complexes (Fig. 1; Burtman & Molnar, 1993; Schwab et al., 2004).

Beneath the Pamir a band of intermediate-depth (50–250 km) earthquakes that extends from the southwestern Pamir northwestward into the central Pamir, bends eastward, and shows diminished earthquake activity beneath the eastern Pamir (Fig. 2; Pegler & Das, 1998; Sippl, Schurr, Yuan, et al., 2013). Receiver function images, seismic tomography, and the analysis of guided waves show that the earthquakes in the western and central Pamir reside in a 10–15 km thick, E- to S-dipping low velocity zone (LVZ) connected to the Asian lithosphere; seismic velocities indicate that the LVZ represents continental crust, constituting, together with the underlying mantle lithosphere, the Asian slab (Schneider et al., 2013; Sippl, Schurr, Tympel, et al., 2013; Mechie et al., 2019). Beneath the northwestern Kunlun, diffuse seismicity at 100–150 km depth was attributed to Tarim lithosphere underthrusting the Pamir (Fan et al., 1994; Pegler & Das, 1998).

Whether Asian lithosphere subducts as a narrow, back-rolling slab of thinned crust (Burtman & Molnar, 1993; Sobel et al., 2013) or whether forceful subduction/delamination of lower crust and mantle lithosphere due to indentation by cratonic Indian mantle lithosphere (Kufner et al., 2016; Metzger et al., 2017) occurs, is debated. This debate impacts on the reconstruction of the India-Asia collision system, the general understanding of continental delamination-, subduction-, and mountain–building-processes, and the assessment of regional-scale fault systems in their geodynamic context.

If an indenter governs the shape of the Pamir orocline, its margins matter. Kufner et al. (2018) argued that a sinistral-oblique transform margin separates indenting cratonic Indian lithosphere beneath the Pamir from subducting Indian continental-margin lithosphere below the Hindu-Kush. The most recent subduction model (Sobel et al., 2013) postulates rollback of a narrow Asian slab with thinned continental crust, involving mantle corner flow and a subduction-transform edge propagator fault separating the subducting Asian slab and its hanging wall from the Tarim block. However, geophysical data indicate that the hinterland crust is not thinned (>50 km; Schneider et al., 2019), questioning the premise of the rollback model. The delamination model (Kufner et al., 2018; Chapman et al., 2017) calls for forced Asian slab subduction due to flat-slab underthrusting of a mechanically-strong Indian continental lithospheric mantle indenter, a process recently modeled for the Pamir (Kelly & Beaumont, 2021). The indenter is imaged by refraction seismology and local body wave tomography as a high velocity zone (HVZ) south of the Asian slab (Mechie et al., 2012; Sippl, Schurr, Tympel, et al., 2013). Teleseismic body and surface wave tomography shows that it connects with the exposed Indian craton (e.g. C. Li et al., 2008; Agius & Lebedev, 2013; van Hinsbergen et al., 2019; Liang et al., 2020); its northern extent has remained unresolved due to the smearing of the indenter HVZ with the HVZ that represents cratonic Asia.

Herein, intermediate-depth earthquakes, focal-mechanism stress data, and a P-wave velocity model derived from new and published local seismological data in companionship with new receiver functions (Xu et al., 2021) illuminate the lithospheric configuration of the central and eastern Pamir and the boundary zone with Tarim. We characterize the northern tip of an indenter—interpreted as a promontory of Indian mantle lithosphere—and its eastern edge, where it abuts on the lithosphere of the Tarim block.

2 Data and Methods

We use seismograms recorded with two new local seismic networks (Text S1 Yuan, Schurr, Bloch, et al., 2018; Yuan, Schurr, Kufner, & Bloch, 2018) and additional regional stations (PMP International (Tajikistan), 2005; SEISDMC, 2021) to detect and locate seismicity in the eastern Pamir (Text S2). Using additional data of an existing earthquake catalog from the western and central Pamir (Sippl, Schurr, Tympel, et al., 2013) we inverted for the 3-dimensional subsurface P-wave velocity structure (Text S3) and jointly relocated seismicity at intermediate depth (Text S4). We determined focal mechanisms of the strongest of the newly located events and inverted for stress directions (Text S5). The resulting seismicity catalog and the velocity structure are published in the Supplemental Material.

3 Seismicity

Crustal seismicity of the upper 30 km is dominated by the aftershock sequences of strong earthquakes that struck the Pamir in 2015/16 and is omitted from the main figures. The middle and lower crust (30–50 km depth) is essentially aseismic (Fig. S3). Intermediate-depth earthquakes in the central and eastern Pamir outline three steeply-dipping, planar to curviplanar segments separated by regions of sparse seismicity (Fig. 2; Fig. 3).

Segment 1 begins at 72.8°E, 38°N, in continuation of the NE-striking, planar seismically active structure farther to the southwest (Fig. 2 Schneider et al., 2013; Sippl, Schurr, Yuan, et al., 2013). It forms an S- to SE-dipping band between 73°E and 74.3°E, and shows vigorous seismicity between 70–180-km-depth in its easternmost part (Fig. 3A; Fig. S2); farther east, seismic activity decreases.

Segment 2 in the eastern Pamir—in the direct continuation of segment 1—contains a few earthquakes at 50–80 km depth in a S-dipping structure (top dotted line in Fig. 3B). Below, at 80-170 km depth, the earthquake-defined band dips N (Fig 2; bottom dotted line in Fig. 3B). Seismicity in segment 2 is less intense compared to segment 1 (Fig. S2). Focal mechanisms of segments 1 and 2 indicate a transpressional stress regime, with the maximum principal stress σ_1 trending N20°W and N12°W, parallel to the surface plate-motion directions, and a vertical σ_3 (Fig. 2).

Seismicity in segment 3 forms a continuous, tentatively ENE-dipping structure at 80–120-km-depth between 37°N and 38°N; it follows the northwestern Kunlun (Fig. 2; Fig. 3C). Seismic activity is comparably weak (Fig. S2). Focal mechanisms indicate transpression with σ_1 trending N7°W, parallel to the surface plate-motion, and a near-vertical σ_3 (Fig. 2).

4 Velocity Structure

In the shallow crust, northeast of the Main Pamir Thrust System (Fig. 3, overview map), the sediment fill of the Tarim basin forms a LVZ (<5 km/s, *TL* in Figs. 3B–D). In the middle–lower crust, the Tarim basement appears as a discontinuous HVZ (6.5–7.5 km/s, *TH* in Fig. 3C, Fig. 3E) at the poorly-resolved rim of the tomographic volume. A LVZ is located in the uppermost mantle of northwestern Tarim (*AL* in Fig. 3G). An arcuate crustal LVZ extends below the northern Pamir, the Kongur Extensional System, and the northwestern Kunlun (5–6 km/s, *PL* in Figs. 3A–C and 3E). It is sandwiched between the Tarim basement HVZ, *TH*, and another crustal HVZ in the central Pamir (6–7 km/s, *PH* in Fig. 3A; Fig. 3E).

At mantle depths, dipping LVZs are located above the seismicity in segments 1–3 (7–8 km/s, *L1*, *L2*, *L3* in Figs. 3A-C and 3F). The LVZs *L2* and *L3* of segments 2 and 3 appear continuous in map view (Fig. 3F), but are separated by the seismicity of segment 2 (Fig. 3B). The seismically active structures are underlain by HVZs (8.5–9.5 km/s, *H1*, *H2*, *H3* in Figs. 3A–C and 3G) and have the same dip as the LVZs above. In segment 1 and 2, the HVZs *H1* and *H2* are continuous along strike below ∼105 km depth (Fig. 3G). In segment 2, the HVZs *H2* and *H3* touch, but are separated by seismicity in the same way as the LVZs *L2* and *L3* (Fig. 3B; Fig. 3G). The LVZs and HVZs of segment 1 (*L1* and *H1*; Fig. 3A) and segment 3 (*L3* and *H3*; Fig. 3C) dip in the same direction as the seismicity structures; those of segment 2 (*L2* and *H2*; Fig. 3B) dip oppositely.

5 Interpretation and Discussion

We visualize our interpretation of the lithospheric architecture of the central and eastern Pamir in the block diagram of Figure 4. Sippl, Schurr, Tympel, et al. (2013) inferred eclogitization of the lower crust of segment 1 due to the sinking of the Asian slab and that this lower crust hosts the band of intermediate-depth earthquakes; in our tomogram, we interpret the LVZ *L1* as the lower crust and the HVZ *H1* as the mantle lithosphere of the Asian slab (Fig. 3A). Upon eclogitization the crust of the slab becomes seismogenic (John et al., 2009) and indistinguishable from the surrounding mantle in terms of seismic velocities (Rondenay et al., 2008). The aseismic mid-crustal LVZ *PL* (Figs. 3A–C and 3E; see also W. Li et al., 2018; Sippl, Schurr, Tympel, et al., 2013), possibly connecting the upper crustal imbrication of the Main Pamir Thrust System with tectonic stacking along shear zones in the middle crust (Fig. 1, cross section), may represent a heated rock volume, developed by excess radiogenic heat production in the thickened crust. Heating due to asthenospheric inflow in the hanging wall of a S-dipping subduction zone is unlikely, as the tomogram does not show a LVZ south of the seismic zone; in contrast, subcrustal P velocities are >8km/s with HVZs (>8.5 km/s) embedded (e.g., *H3*), indicating relatively cold and rigid lithospheric mantle south of the Asian slab.

Segment 2 appears to be the eastern continuation of segment 1 of the Asian slab because of the similar depth extent of the seismic zone and the continuity of the underlying HVZ (Fig. 2; Figs. 3A, 3B, and 3G). The seismically active structure is overturned below ∼80 km depth (Fig. 2; Fig. 3B). A tear likely separates segments 1 and 2 because of the short (∼40 km) distance across which the slab dip changes and the separating seismicity gap. The Asian slab terminates in a seismicity cluster below the Kashgar-Yecheng Transfer System at 76.2°E (Fig. 2), where it is presumably torn off Tarim's lithosphere to the east. The dip beyond vertical of segment 2 shows that a force acts normal to the slab and hints towards the presence of an indenter. In an alternative configuration, in which segment 2 forms a continuous, N-dipping unit with segment 3, the along-strike correlation of seismicity and the velocity structures around 38°N, between 73°E and 76°E would be coincidental and we could not interpret the ∼ENE-dipping velocity- and Moho-structures (see below; Xu et al., 2021), so that we reject this interpretation.

For segments 1–3, σ_1 at depth is parallel to the ∼NNW-oriented surface velocity of the Pamir crust (e.g. Zubovich et al., 2010; Ischuk et al., 2013; Metzger et al., 2020). The subhorizontal σ_1 indicates that a NNW–SSE compressive stress field governs the deep structure of the Pamir, which favors a pushing indenter. In contrast, N–S extension should occur S of the slab if deformation below the Pamir was governed by a narrow Asian slab rolling back northward. Parallelism of the surface motion with σ_1 at depth implies that the lithospheric mantle is coupled to the crust. For segments 1 and 2 it arises if collision occurs at an indenter tip.

In concert with the lack of thinned hinterland crust (Schneider et al., 2019) and the imaging of a HVZ at ∼200 km depth that connects with the exposed Indian craton below the Pamir-Karakorum (C. Li et al., 2008; Agius & Lebedev, 2013; van Hinsbergen et al., 2019), the following of our observations support the presence of an indenter below the Pamir: (1) the repeated detection of HVZ *H3* south of the Asian slab (this study; Mechie et al., 2012; Sippl, Schurr, Tympel, et al., 2013) that excludes asthenospheric inflow above a S-dipping, back-rolling subduction zone; (2) the overturned dip of the seismic plane of segment 2, testified by a change in dip of seismicity in profile view and by along-strike correlation with segment 1; (3) the NNW–SSE compressive stress field across the central and eastern Pamir at mantle depth (50 - 100 km) that is coupled with surface motion.

The indenter is most likely cratonic Indian lithosphere, because the lithosphere of the central and southern Pamir terranes would be too weak to transmit enough force to delaminate and overturn the Asian slab (Kelly & Beaumont, 2021). We locate the delamination front at the base of the rheologically weak mid-crustal LVZ *PL* (red line in Fig. 4). The present location and form of the Pamir and the Asian slab is in this interpretation governed by the shape of the indenter. Additional structural complexity, such as the location of slab tears or turn-overs, may be due to lateral changes in the strength of the indented Asian lithosphere or the along-strike variability of the indenter tip (Z.-H. Li et al., 2016; Kelly & Beaumont, 2021). For example, the mid-crustal HVZ *PH*, which overlies a distinctive Moho bulge in segment 1 (Fig 3A; Schneider et al., 2019), may represent a lithosphere-scale anticline; in segment 1, the top of the indenter appears to rise higher than in segment 2 and in particular in segment 3 (Fig. 4).

In the northwestern Kunlun, the seismicity band of segment 3, the LVZ *L3*, and the HVZ *H3* as well as the Moho conversion (Xu et al., 2021) dip ∼ENE, indicating that Pamir crust and indenter mantle lithosphere underthrust the Asian mantle lithosphere (Fig. 3C). The earthquakes may, as in the Asian slab, occur in thickened crust undergoing eclogitization. This crust is dragged to depth between the bulldozing indenter and the margin of the Tarim block. The stress field of the earthquakes inside the underthrusting crust *L3* indicates that it moves with the NNW-ward moving indenter. Earthquake focal mechanisms and the orientation of σ_1 in segment 3 testifies that underthrusting is highly oblique with respect to Tarim hanging wall. As the tomographic and receiver function Moho both dip ∼WSW beneath the northwestern Kunlun east of LVZ *L3* (Fig. 3C; Xu et al., 2021), we infer that Tarim underthrusts the northwestern Kunlun as well, building an interlaced stack of (from top to bottom) Kunlun–Tarim–Pamir crust (Fig. 4C). This excess crust may be responsible for a positive anomaly in the isostatic gravity residual (20-mGal-contour in Fig. 2; Balmino et al., 2012) that flanks the northern edge of the Tibet plateau (Fig. 2, inset), and was interpreted to represent thrusting of Tarim crust under the western and central Kunlun (Wittlinger et al., 2004).

The transpressive stress field of the deep seismic zone (segment 3) outlines a compressive lithospheric transform zone as the deep plate boundary between the Indian indenter and the Tarim block. It changes to a forced subduction/delamination boundary due to indentation under the central Pamir. The tear that separates the Asian slab from Tarim propagates northward with the advancing indenter. Indentation may have caused the capture and dragging along of the crust from the collision system into the transform zone (Fig. 4C). The transform margin likely transitions southeastward into a subduction plate boundary where the Tarim block underthrusts the western Tibet plateau. Our interpretation of the deep structure suggests a strong along-strike segmentation of the northern tip of the Indian plate; it subducts under the Hindu Kush (Kufner et al., 2021), indents in the Pamir (this study), and has variable dip angles and locations in the rest of Tibet (e.g. Zhao et al., 2010).

6 Conclusion

We located zones of intermediate-depth seismicity in the eastern Pamir and northwestern Kunlun, established their geometries, determined the principal stress orientations, and computed a seismic velocity model of the subsurface. We traced a subducting/delaminating Asian slab eastward as far as the western edge of the Tarim block and showed that the eastern segment of the slab is overturned and torn from the central one. Together with the presence of a high velocity zone in front of the slab and the parallelism of the largest principal stress at depth with surface motion across the eastern and central Pamir, this geometry indicates underthrusting of Indian mantle lithosphere beneath the Pamir and delamination of the Asian slab. A slice of lower crust is dragged along with the indenter and smeared into the compressive transform boundary with the Tarim block at depth.

Acknowledgments

We thank the drivers and field participants from the Institute of Tibetan Plateau Research, especially Hongbing Liu, who helped to organize the station deployment, and Christian Sippl for sharing code and discussion. Funded by the CaTeNA project of the German Federal Ministry of Science and Education (support codes 03G0878A and 03G0878B). Seismic data was handled using *obspy* (Krischer et al., 2015) and *pyrocko* (Heimann et al., 2017). Figures were created with the help of the *Generic Mapping Tools* (Wessel et al., 2013) and *maplotlib* (Hunter, 2007). Part of the instruments were provided by GIPP of GFZ Potsdam. Seismic data are archived by GEOFON data center.

References

Agius, M. R., & Lebedev, S. (2013). Tibetan and indian lithospheres in the upper mantle beneath tibet: Evidence from broadband surface-wave dispersion. *Geochemistry, Geophysics, Geosystems*, *14*(10), 4260–4281.

Balmino, G., Vales, N., Bonvalot, S., & Briais, A. (2012). Spherical harmonic modelling to ultra-high degree of bouguer and isostatic anomalies. *Journal of Geodesy*, *86*(7), 499–520.

Burtman, V. S., & Molnar, P. H. (1993). *Geological and geophysical evidence for* *deep subduction of continental crust beneath the pamir* (Vol. 281). Geological Society of America.

Chapman, J. B., Carrapa, B., Ballato, P., DeCelles, P. G., Worthington, J., Oimahmadov, I., ... Ketcham, R. (2017). Intracontinental subduction beneath the pamir mountains: Constraints from thermokinematic modeling of shortening in the tajik fold-and-thrust belt. *GSA Bulletin*, *129*(11-12), 1450–1471.

Fan, G., Ni, J. F., & Wallace, T. C. (1994). Active tectonics of the pamirs and karakorum. *Journal of Geophysical Research: Solid Earth*, *99*(B4), 7131–7160.

Heimann, S., Kriegerowski, M., Isken, M., Cesca, S., Daout, S., Grigoli, F., ... others (2017). Pyrocko-an open-source seismology toolbox and library. *GFZ Data Services*. doi: 10.5880/GFZ.2.1.2017.001

Hunter, J. D. (2007). Matplotlib: A 2d graphics environment. *Computing in Science & Engineering*, *9*(3), 90–95. doi: 10.1109/MCSE.2007.55

Ischuk, A., Bendick, R., Rybin, A., Molnar, P., Khan, S. F., Kuzikov, S., ... others (2013). Kinematics of the pamir and hindu kush regions from gps geodesy. *Journal of geophysical research: solid earth*, *118*(5), 2408–2416.

John, T., Medvedev, S., Rüpke, L. H., Andersen, T. B., Podladchikov, Y. Y., & Austrheim, H. (2009). Generation of intermediate-depth earthquakes by self-localizing thermal runaway. *Nature Geoscience*, *2*(2), 137–140.

Kelly, S., & Beaumont, C. (2021). Balanced cross-sections and numerical modeling of the lithospheric-scale evolution of the hindu kush and pamir. *Journal of Geophysical Research: Solid Earth*, *126*(3), e2020JB020678.

Krischer, L., Megies, T., Barsch, R., Beyreuther, M., Lecocq, T., Caudron, C., & Wassermann, J. (2015). Obspy: A bridge for seismology into the scientific python ecosystem. *Computational Science & Discovery*, *8*(1), 014003.

Kufner, S.-K., Kakar, N., Bezada, M., Bloch, W., Metzger, S., Yuan, X., ... others (2021). The hindu kush slab break-off as revealed by deep structure and crustal deformation. *Nature communications*, *12*(1), 1–11.

Kufner, S.-K., Schurr, B., Ratschbacher, L., Murodkulov, S., Abdulhameed, S., Ischuk, A., ... Kakar, N. (2018). Seismotectonics of the tajik basin and surrounding mountain ranges. *Tectonics*, *37*(8), 2404–2424.

Kufner, S.-K., Schurr, B., Sippl, C., Yuan, X., Ratschbacher, L., Ischuk, A., ... others (2016). Deep india meets deep asia: Lithospheric indentation, delamination and break-off under pamir and hindu kush (central asia). *Earth and Planetary Science Letters*, *435*, 171–184.

Li, C., Van der Hilst, R. D., Meltzer, A. S., & Engdahl, E. R. (2008). Subduction of the indian lithosphere beneath the tibetan plateau and burma. *Earth and Planetary Science Letters*, *274*(1-2), 157–168.

Li, W., Chen, Y., Yuan, X., Schurr, B., Mechie, J., Oimahmadov, I., & Fu, B. (2018). Continental lithospheric subduction and intermediate-depth seismicity: Constraints from s-wave velocity structures in the pamir and hindu kush. *Earth and Planetary Science Letters*, *482*, 478–489.

Li, Z.-H., Liu, M., & Gerya, T. (2016). Lithosphere delamination in continental collisional orogens: A systematic numerical study. *Journal of Geophysical Research: Solid Earth*, *121*(7), 5186–5211.

Liang, Y., Li, L., Liao, J., & Gao, R. (2020). Interaction of the indian and asian plates under the pamir and hindu-kush regions: Insights from 3-d shear wave velocity and anisotropic structures. *Geochemistry, Geophysics, Geosystems*, *21*(8), e2020GC009041.

Lu, S., Li, H., Zhang, C., & Niu, G. (2008). Geological and geochronological evidence for the precambrian evolution of the tarim craton and surrounding continental fragments. *Precambrian Research*, *160*(1-2), 94–107.

Mechie, J., Schurr, B., Yuan, X., Schneider, F., Sippl, C., Minaev, V., ... others (2019). Observations of guided waves from the pamir seismic zone provide additional evidence for the existence of subducted continental lower crust.

Tectonophysics, *762*, 1–16.
Mechie, J., Yuan, X., Schurr, B., Schneider, F., Sippl, C., Ratschbacher, L., … others (2012). Crustal and uppermost mantle velocity structure along a profile across the pamir and southern tien shan as derived from project tipage wide-angle seismic data. *Geophysical Journal International*, *188*(2), 385–407.
Metzger, S., Ischuk, A., Deng, Z., Ratschbacher, L., Perry, M., Kufner, S.-K., … Moreno, M. (2020). Dense gnss profiles across the northwestern tip of the india-asia collision zone: Triggered slip and westward flow of the peter the first range, pamir, into the tajik depression. *Tectonics*, *39*(2), e2019TC005797.
Metzger, S., Schurr, B., Ratschbacher, L., Sudhaus, H., Kufner, S.-K., Schöne, T., … Bendick, R. (2017). The 2015 mw7. 2 sarez strike-slip earthquake in the pamir interior: Response to the underthrusting of india's western promontory. *Tectonics*, *36*(11), 2407–2421.
Pegler, G., & Das, S. (1998). An enhanced image of the pamir–hindu kush seismic zone from relocated earthquake hypocentres. *Geophysical Journal International*, *134*(2), 573–595.
PMP International (Tajikistan). (2005). *Tajikistan national seismic network.* International Federation of Digital Seismograph Networks. Retrieved from `http://www.fdsn.org/doi/10.7914/SN/TJ` doi: 10.7914/SN/TJ
Rondenay, S., Abers, G. A., & Van Keken, P. E. (2008). Seismic imaging of subduction zone metamorphism. *Geology*, *36*(4), 275–278.
Schneider, F., Yuan, X., Schurr, B., Mechie, J., Sippl, C., Haberland, C., … others (2013). Seismic imaging of subducting continental lower crust beneath the pamir. *Earth and Planetary Science Letters*, *375*, 101–112.
Schneider, F., Yuan, X., Schurr, B., Mechie, J., Sippl, C., Kufner, S.-K., … others (2019). The crust in the pamir: Insights from receiver functions. *Journal of Geophysical Research: Solid Earth*, *124*(8), 9313–9331.
Schwab, M., Ratschbacher, L., Siebel, W., McWilliams, M., Minaev, V., Lutkov, V., … others (2004). Assembly of the pamirs: Age and origin of magmatic belts from the southern tien shan to the southern pamirs and their relation to tibet. *Tectonics*, *23*(4).
SEISDMC. (2021). Data management centre of the china national seismic network at the institute of geophysics. *China Earthquake Administration*. doi: 10.11998/SeisDmc/SN
Sippl, C., Schurr, B., Tympel, J., Angiboust, S., Mechie, J., Yuan, X., … others (2013). Deep burial of asian continental crust beneath the pamir imaged with local earthquake tomography. *Earth and Planetary Science Letters*, *384*, 165–177.
Sippl, C., Schurr, B., Yuan, X., Mechie, J., Schneider, F., Gadoev, M., … others (2013). Geometry of the pamir-hindu kush intermediate-depth earthquake zone from local seismic data. *Journal of Geophysical Research: Solid Earth*, *118*(4), 1438–1457.
Sobel, E. R., Chen, J., Schoenbohm, L. M., Thiede, R., Stockli, D. F., Sudo, M., & Strecker, M. R. (2013). Oceanic-style subduction controls late cenozoic deformation of the northern pamir orogen. *Earth and Planetary Science Letters*, *363*, 204–218.
van Hinsbergen, D. J., Lippert, P. C., Li, S., Huang, W., Advokaat, E. L., & Spakman, W. (2019). Reconstructing greater india: Paleogeographic, kinematic, and geodynamic perspectives. *Tectonophysics*, *760*, 69–94.
Wessel, P., Smith, W. H., Scharroo, R., Luis, J., & Wobbe, F. (2013). Generic mapping tools: improved version released. *Eos, Transactions American Geophysical Union*, *94*(45), 409–410.
Wittlinger, G., Vergne, J., Tapponnier, P., Farra, V., Poupinet, G., Jiang, M., … Paul, A. (2004). Teleseismic imaging of subducting lithosphere and moho offsets beneath western tibet. *Earth and Planetary Science Letters*, *221*(1-4),

117–130.

Xu, Q., Zhao, J., Yuan, X., Liu, H., Ju, C., Schurr, B., & Bloch, W. (2021). Deep crustal contact between the pamir and tarim basin deduced from receiver functions. *Geophysical Research Letters*.

Yuan, X., Schurr, B., Bloch, W., Xu, Q., & Zhao, J. (2018). East pamir seismic network. *GFZ Data services*. doi: 10.14470/3U7560589977

Yuan, X., Schurr, B., Kufner, S.-K., & Bloch, W. (2018). Sarez pamir aftershock seismic network. *GFZ Data services*. doi: 10.14470/4U7561589984

Zhao, J., Yuan, X., Liu, H., Kumar, P., Pei, S., Kind, R., ... others (2010). The boundary between the indian and asian tectonic plates below tibet. *Proceedings of the National Academy of Sciences*, *107*(25), 11229–11233.

Zubovich, A. V., Wang, X.-q., Scherba, Y. G., Schelochkov, G. G., Reilinger, R., Reigber, C., ... others (2010). Gps velocity field for the tien shan and surrounding regions. *Tectonics*, *29*(6).

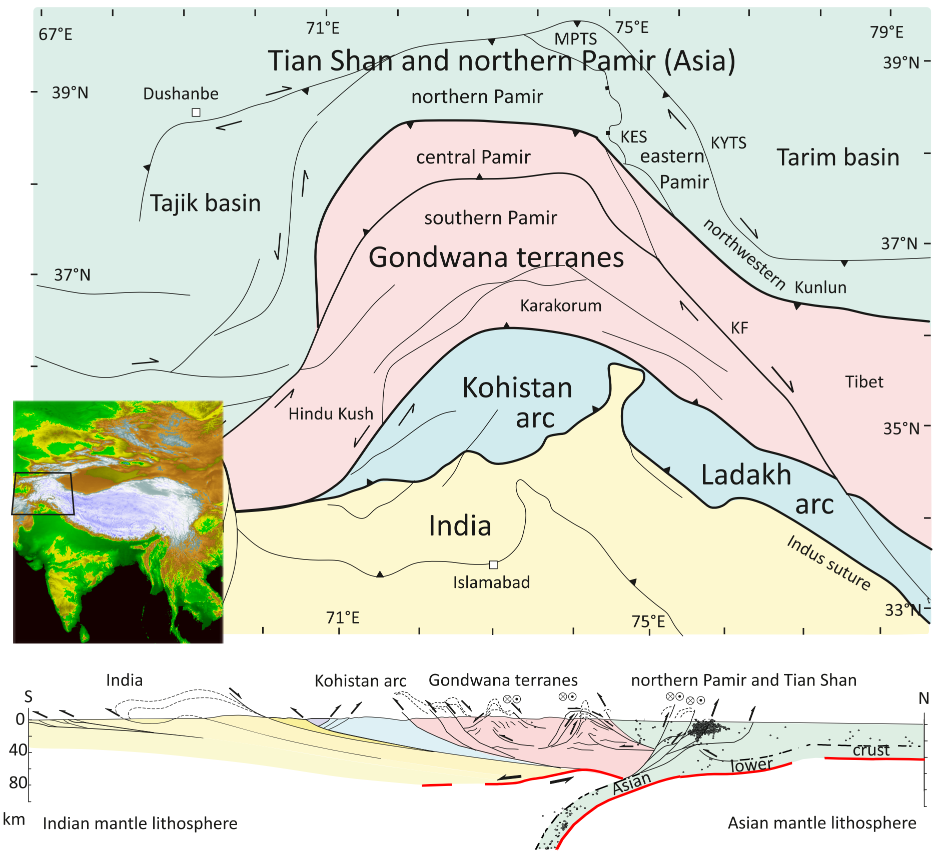

Figure 1. Tectonic units of the Pamir in map view and as a schematic cross section along ∼74°E. MPTS: Main Pamir Thrust System; KYTS: Kashgar-Yecheng Transfer System; KES: Kongur Extensional System; KF: Karakorum Fault.

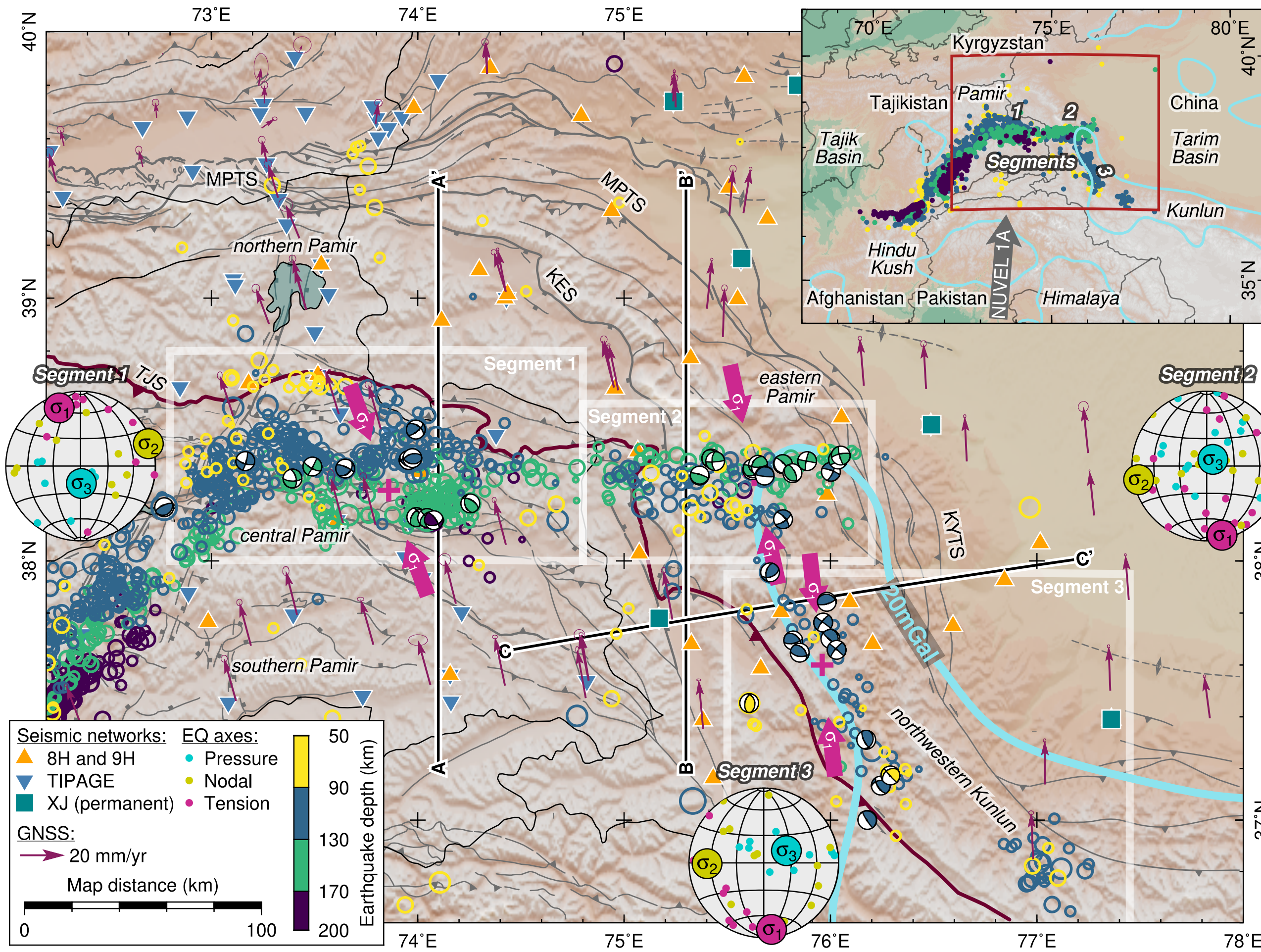

Figure 2. Seismotectonic map of the Pamir and northwestern Kunlun with seismic networks, seismicity, focal mechanisms, principal stress directions, earthquake P-, T-, N-axes, global navigation satellite system (GNSS) velocity field (Ischuk et al., 2013; Zubovich et al., 2010), and 20mGal positive isostatic gravity anomaly (Balmino et al., 2012). TJS, Tanymas-Jinsha suture.

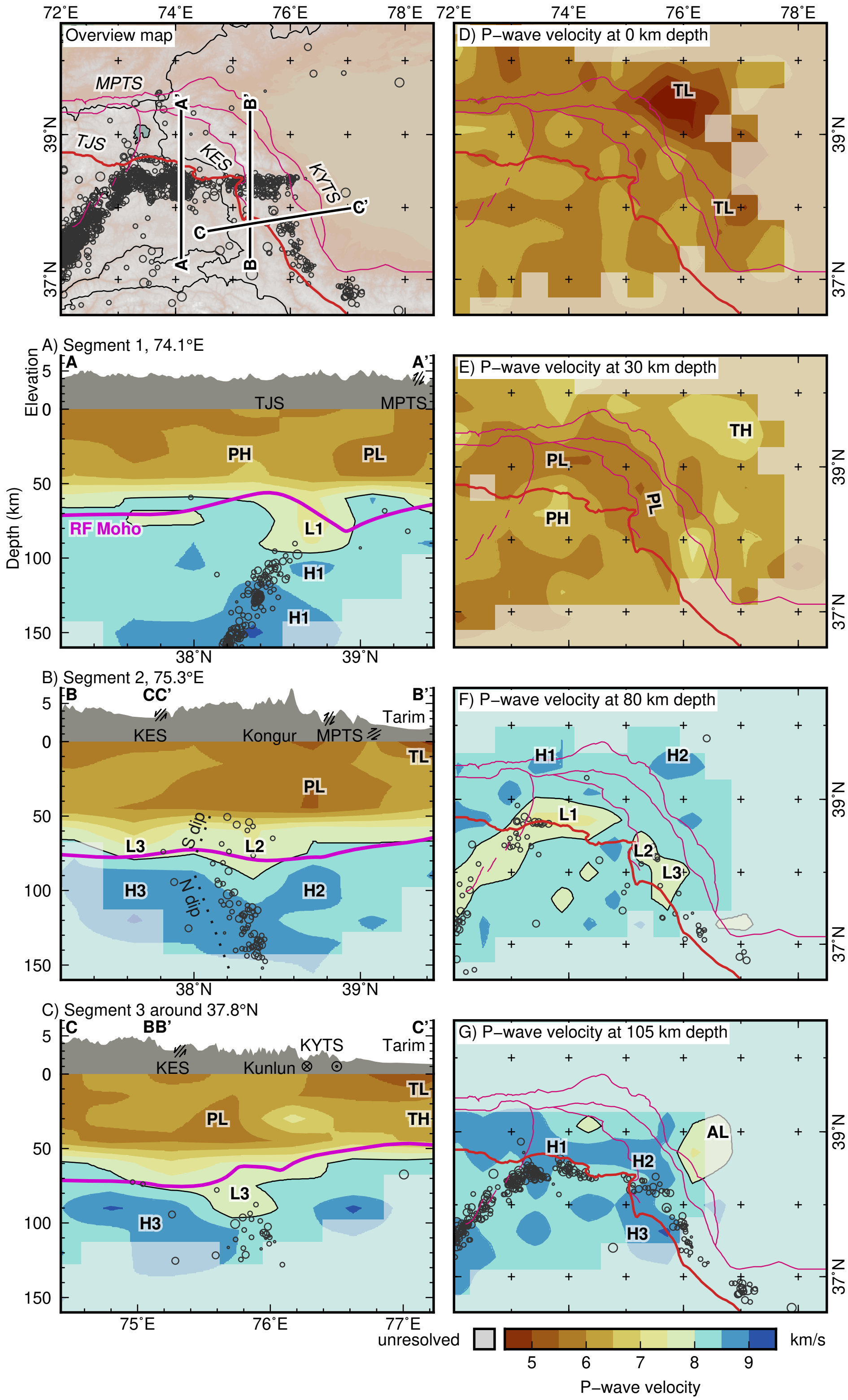

Figure 3. Sections through the tomogram. A-C) Profiles shown on overview map. Magenta: Receiver function Moho (Schneider et al., 2019; Xu et al., 2021). D-G) Horizontal sections. *TH*, *PH*, *H1*, *H2*, *H3*: high velocity zones. *TL*, *PL*, *L1*, *L2*, *L3*, *AL*: low velocity zones.

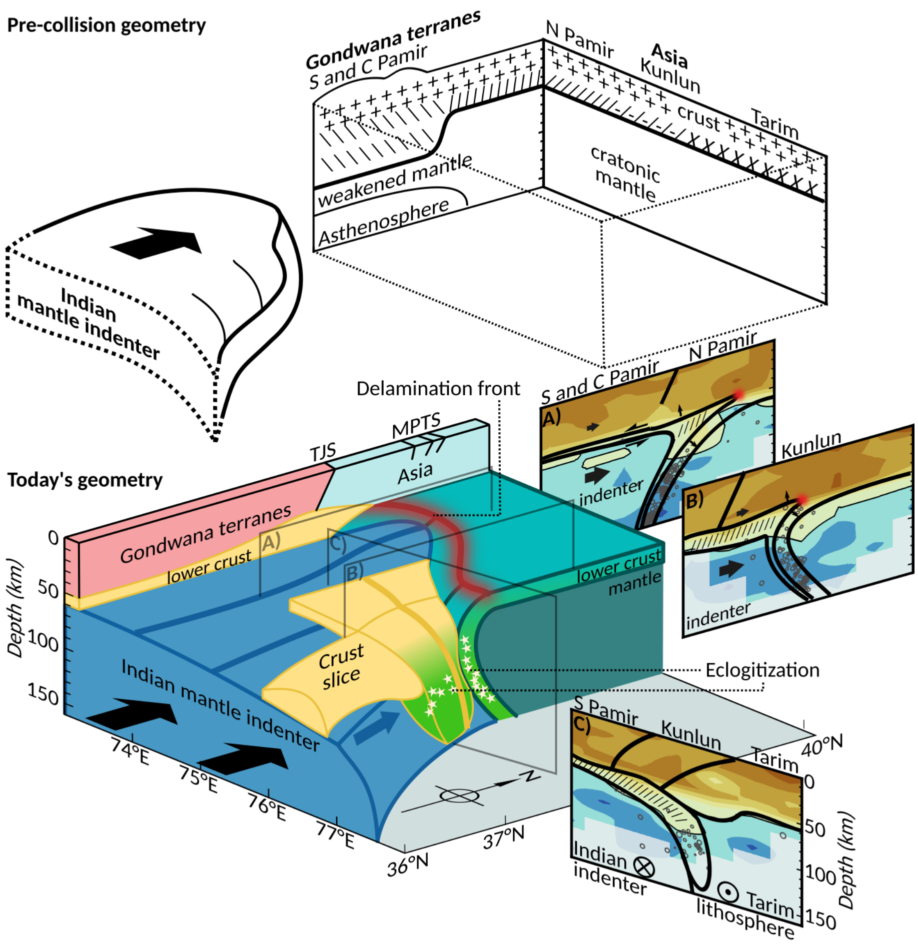

Figure 4. Top: pre-collision geometry. Bottom: interpreted block diagram of the deep lithospheric structure beneath the Pamir and northwestern Kunlun. A-C) Interpreted cross sections of Fig. 3. '///' symbols mark the lower crust involved in the collision process.

Supporting Information for "Structure of the deep lithosphere between Pamir and Tarim"

Wasja Bloch[1], Bernd Schurr[1], Xiaohui Yuan[1], Lothar Ratschbacher[2],

Sanaa Reuter[2], Sofia-Katerina Kufner[1,3], Qiang Xu[4,5], Junmeng Zhao[4,5]

[1]GFZ German Research Centre for Geosciences, 14473 Potsdam, Germany

[2]Geologie, Technische Universität Bergakademie Freiberg, 09599 Freiberg, Germany

[3]British Antarctic Survey, Cambridge CB3 0ET, England

[4]Key Laboratory of Continental Collision and Plateau Uplift, Institute of Tibetan Plateau Research, Chinese Academy of Sciences, Beijing 100101, China

[5]CAS Center for Excellence in Tibetan Plateau Earth Sciences, Beijing 100101, China

Contents of this file

1. Text S1 to Text S4
2. Figure S1 to Figure S6

Additional Supporting Information (Files uploaded separately)

1. Captions for Datasets S1 to S4

Corresponding author: Wasja Bloch, Section Lithosphere Dynamics, German Geoscience Centre GFZ, Telegrafenberg, Potsdam, Germany. (wasja@gfz-potsdam.de)

Introduction This supporting information gives details of the processing steps briefly described in the main article. Additional figures allowing to understand seismic network sensitivity, as well as performance and stability of the 3-dimensional velocity model are presented. The seismic event catalog, seismic wave speed model, and phase arrival time picks are published as separate data files and briefly described here.

Text S1. Data

We operated the East Pamir seismic network (FDSN code 8H; Yuan, Schurr, Bloch, et al., 2018) with 30 sites in the eastern Pamir, northwestern Kunlun, and northwestern Tarim basin between August 2015 and July 2017, and the Sarez-Pamir aftershock seismic network (FDSN code 9H Yuan, Schurr, Kufner, & Bloch, 2018) with 10 sites in the central Pamir between February 2016 and July 2017. We used additional seismic waveform data from the Xinjiang regional seismic network (XJ; SEISDMC, 2021) and the Tajik National Seismic Network (FDSN network code TJ; SEISDMC, 2021).

Text S2. Seismic Event Detection, Phase Picking, and Initial Localization

We detected 39,309 seismic events using the *Lassie* earthquake detector (Comino et al., 2017), 10,900 of which at intermediate depth (>50 km), and automatically picked P-wave arrival times with *MannekenPix* (Aldersons, 2004) and S-wave arrival times with *spicker* (Diehl et al., 2009). After each arrival time picking run, events were located with *hypo71* (Lee & Lahr, 1972), and picks with the highest residuals were removed subsequently until the location root-mean-square misfit fell below a threshold of 2-s for P-waves only and 3-s for P- and S-waves combined. We then used a subset of 1,855 seismic events with best constrained arrival-time picks to invert for a depth-dependent 1-D velocity model and static station corrections using *velest* (Kissling et al., 1994). We again relocated all events in this model and removed those arrival times that yielded a residual 5 times larger than the standard deviation of all residuals of a certain seismic phase on a certain station. In total, we located 29,795 seismic events in the crust and in the mantle.

Text S3. Inversion for the Subsurface Velocity Field

To derive a dataset suitable for tomographic inversion we augmented the catalog with events from Sippl et al. (2013) and used a spatially declustered set of 2,264 events from the combined catalog with a total of 38,423 well-constrained P- and 15,910 S-arrival times. Inversion for the 3-D subsurface P-wave velocity structure was conducted using *simulps* (Thurber, 1983).

The seismic velocity field was parameterized as gradients between a rectangular grid of fixed nodes. After testing of various node configurations, we used a node spacing of 40-km in horizontal and 15-km in vertical direction (Figs. S1a and S3). The 1-D starting model was found by first inverting for the 1-D velocity gradients between vertical nodes and station corrections. Then, we constrained the velocities to increase with depth and that they do not exceed the velocity at 75-km depth (Fig. S1a). The model space was explored with various damping parameters (Fig. S1b) and the final model was found by first inverting solely for the velocity structure and earthquake parameters, and then allowing for minor adjustments by letting non-modeled residuals be taken up by station corrections. A checkerboard resolution test was used to assess the sensitivity of the model and mask poorly resolved regions (Fig. S3).

Text S4. Relocalization

To focus on sub-crustal processes we discarded crustal earthquakes (<50-km depth), which were dominated by a strong earthquake sequence and are confined to the upper ∼40-km depth. We added intermediate depth earthquakes with at least 4 S-picks that were previously excluded from the tomographic inversion. We then relocated all events with the *hypoDD* algorithm (Waldhauser & Ellsworth, 2000), yielding a unified catalog of

1,493 events at intermediate depth, consisting of newly detected events in the eastern and central Pamir and previously reported events from the western and central Pamir (Sippl et al., 2013).

Text S5. Focal Mechanisms and Stress Directions

For 30 events, we estimated focal mechanisms using P-wave first motion polarities and P-to-S amplitude ratios using the *HASH* algorithm (Hardebeck & Shearer, 2003; Bloch et al., 2018), and added 9 moment tensors of Kufner et al. (2016). For the three spatially clearly separated seismicity segments we inverted for the principal stress directions using the *slick* algorithm (Gephart & Forsyth, 1984).

Data Set S1.

Bloch_et-al_2021_seismic_event_catalog.dat

The seismic event catalog presented in the main article.

Seismic events from years 2008-2010 are relocated from Sippl et al. (2013)

Data Set S2.

velocity_model.zip

Folder containing the nodes of the tomographic velocity model and scripts to extract and plot the published and custom profiles.

Data Set S3. "EQKS" input file to *simulps* (Thurber, 1983) used to compute the velocity model.

See Evans, Eberhart-Phillips, and Thurber (1994) Unit04, for definitions.

Phase picks from years 2008-2010 are from Sippl et al. (2013)

Data Set S4.

"hypoDD.pha" input file to *hypoDD* (Waldhauser & Ellsworth, 2000) used to relocate the seismic events.

See Waldhauser (2001) for definitions

Phase picks from years 2008-2010 are from Sippl et al. (2013)

References

Aldersons, F. (2004). Toward three-dimensional crustal structure of the dead sea region from local earthquake tomography. *PhD thesis*.

Bloch, W., Schurr, B., Kummerow, J., Salazar, P., & Shapiro, S. A. (2018). From slab coupling to slab pull: Stress segmentation in the subducting nazca plate. *Geophysical*

Research Letters, *45*(11), 5407–5416.

Comino, J. Á. L., Heimann, S., Cesca, S., Milkereit, C., Dahm, T., & Zang, A. (2017). Automated full waveform detection and location algorithm of acoustic emissions from hydraulic fracturing experiment. *Procedia engineering*, *191*, 697–702.

Diehl, T., Deichmann, N., Kissling, E., & Husen, S. (2009). Automatic s-wave picker for local earthquake tomography. *Bulletin of the Seismological Society of America*, *99*(3), 1906–1920.

Evans, J. R., Eberhart-Phillips, D., & Thurber, C. (1994). *User's manual for simulps12 for imaging vp and vp/vs; a derivative of the" thurber" tomographic inversion simul3 for local earthquakes and explosions* (Tech. Rep.). US Geological Survey,.

Gephart, J. W., & Forsyth, D. W. (1984). An improved method for determining the regional stress tensor using earthquake focal mechanism data: application to the san fernando earthquake sequence. *Journal of Geophysical Research: Solid Earth*, *89*(B11), 9305–9320.

Hardebeck, J. L., & Shearer, P. M. (2003). Using s/p amplitude ratios to constrain the focal mechanisms of small earthquakes. *Bulletin of the Seismological Society of America*, *93*(6), 2434–2444.

Kissling, E., Ellsworth, W., Eberhart-Phillips, D., & Kradolfer, U. (1994). Initial reference models in local earthquake tomography. *Journal of Geophysical Research: Solid Earth*, *99*(B10), 19635–19646.

Kufner, S.-K., Schurr, B., Sippl, C., Yuan, X., Ratschbacher, L., Ischuk, A., … others (2016). Deep india meets deep asia: Lithospheric indentation, delamination and break-off under pamir and hindu kush (central asia). *Earth and Planetary Science Letters*, *435*, 171–184.

Lee, W. H. K., & Lahr, J. C. (1972). *Hypo71: A computer program for determining hypocenter, magnitude, and first motion pattern of local earthquakes.* US Department of the Interior, Geological Survey, National Center for ....

SEISDMC. (2021). Data management centre of the china national seismic network at the institute of geophysics. *China Earthquake Administration*. doi: 10.11998/SeisDmc/SN

Sippl, C., Schurr, B., Tympel, J., Angiboust, S., Mechie, J., Yuan, X., ... others (2013). Deep burial of asian continental crust beneath the pamir imaged with local earthquake tomography. *Earth and Planetary Science Letters*, *384*, 165–177.

Thurber, C. H. (1983). Earthquake locations and three-dimensional crustal structure in the coyote lake area, central california. *Journal of Geophysical Research: Solid Earth*, *88*(B10), 8226–8236.

Waldhauser, F. (2001). hypodd–a program to compute double-difference hypocenter locations.

doi: 10.7916/D8SN072H

Waldhauser, F., & Ellsworth, W. L. (2000). A double-difference earthquake location algorithm: Method and application to the northern hayward fault, california. *Bulletin of the Seismological Society of America*, *90*(6), 1353–1368.

Yuan, X., Schurr, B., Bloch, W., Xu, Q., & Zhao, J. (2018). East pamir seismic network. *GFZ Data services*. doi: 10.14470/3U7560589977

Yuan, X., Schurr, B., Kufner, S.-K., & Bloch, W. (2018). Sarez pamir aftershock seismic network. *GFZ Data services*. doi: 10.14470/4U7561589984

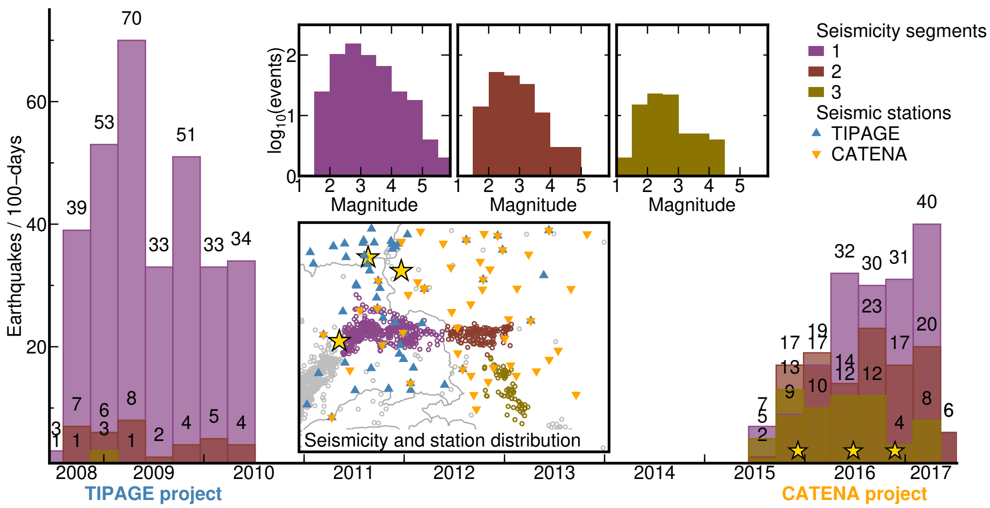

Figure S1. Seismicity rate, local event magnitudes, and station distribution for the three seismicity segments discussed in the main article. Stations of the TIPAGE project (2008-2010, blue) were located in the Tajik Pamir and covered the central segment. Stations of the CATENA project (2015-2017, orange), including networks 8H, 9H and XJ, were located in the Chinese Pamir and Tarim basin and covered the eastern and south-eastern segment. Additional stations were placed in the Tajik Pamir in February 2016. Aftershock sequences of strong earthquakes (stars) in December 2015, June 2016, and November 2016 represent seismic noise that lowered the detection capability of intermediate depth seismicity. Magnitudes of events that occur outside one of the networks (especially in the south-eastern segment) tend to be overestimated. Event rate in the central segment is significantly higher compared to the eastern and south-eastern segment, despite the different network configuration and noise conditions.

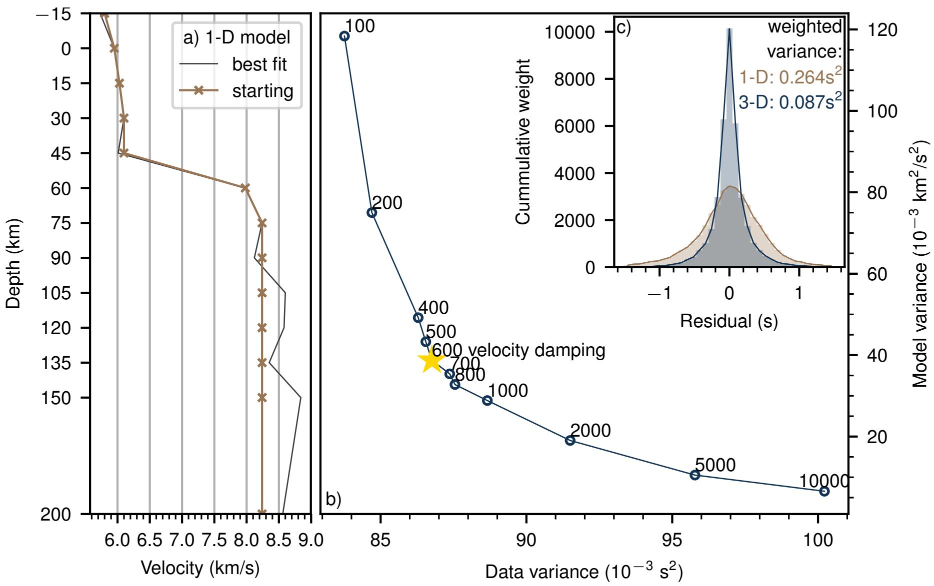

Figure S2. a) 1D models. Best fit: Minimum misfit model after 1-D inversion with *simulps* with station corrections. Starting: Starting model for the 3D inversion. We applied a positivity and a maximum velocity constraint to avoid pre-defining such essential structures in the 3-D inversion b) L-curve to find optimal velocity damping parameter. Star: chosen value c) Reduction of arrival time residuals and variance from 1-D starting model to the presented 3-D model.

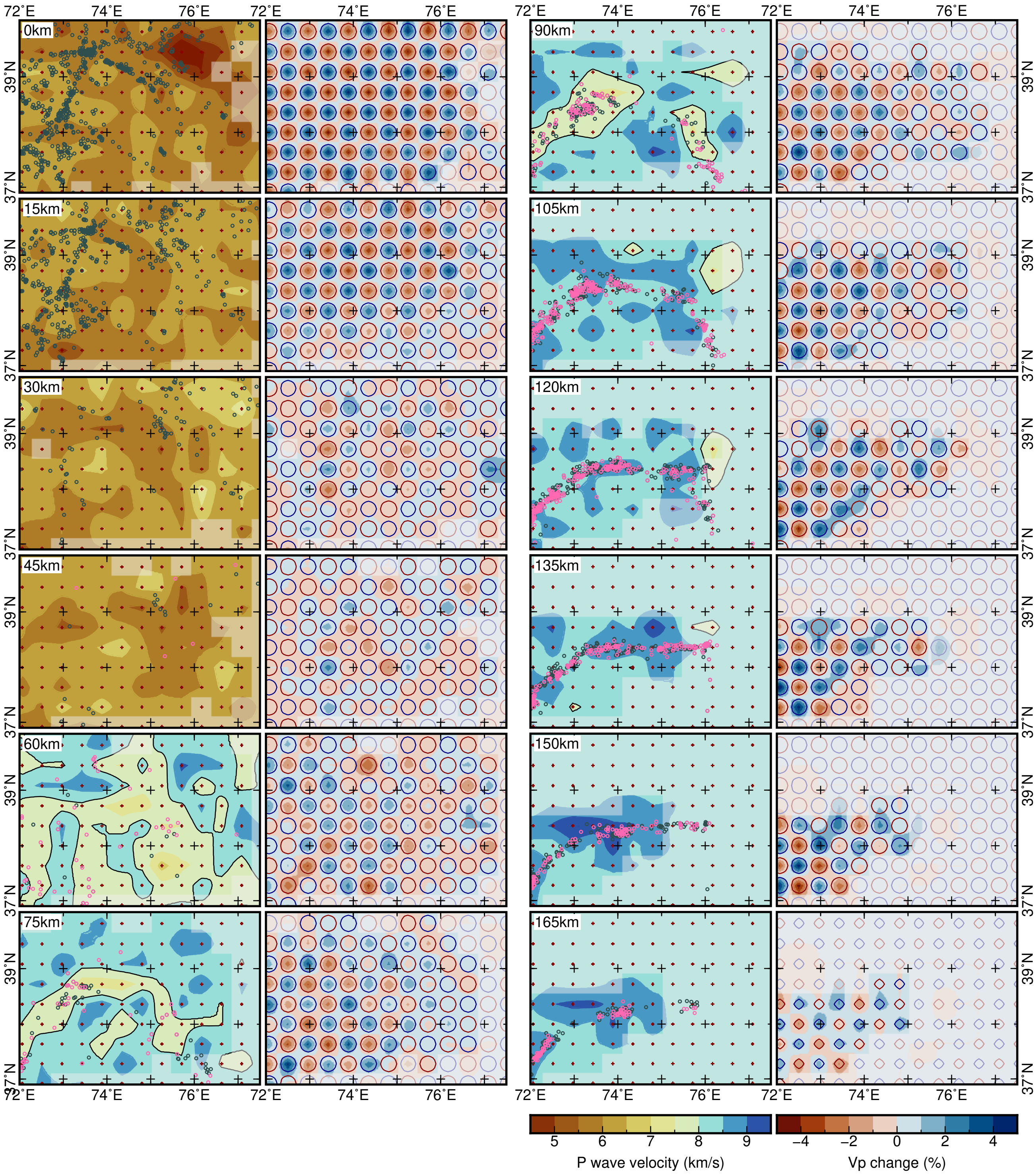

Figure S3. Horizontal slices through the tomogram at the node planes. Columns 1 and 3: Seismic velocities (colored background), grid nodes (red crosses), earthquakes used for tomographic inversion (gray circles), relocated earthquakes at intermediate depth (pink circles). Columns 2 and 4: Results of checkerboard recovery test: recovered model (colored background), input model (+/- 1% contours).

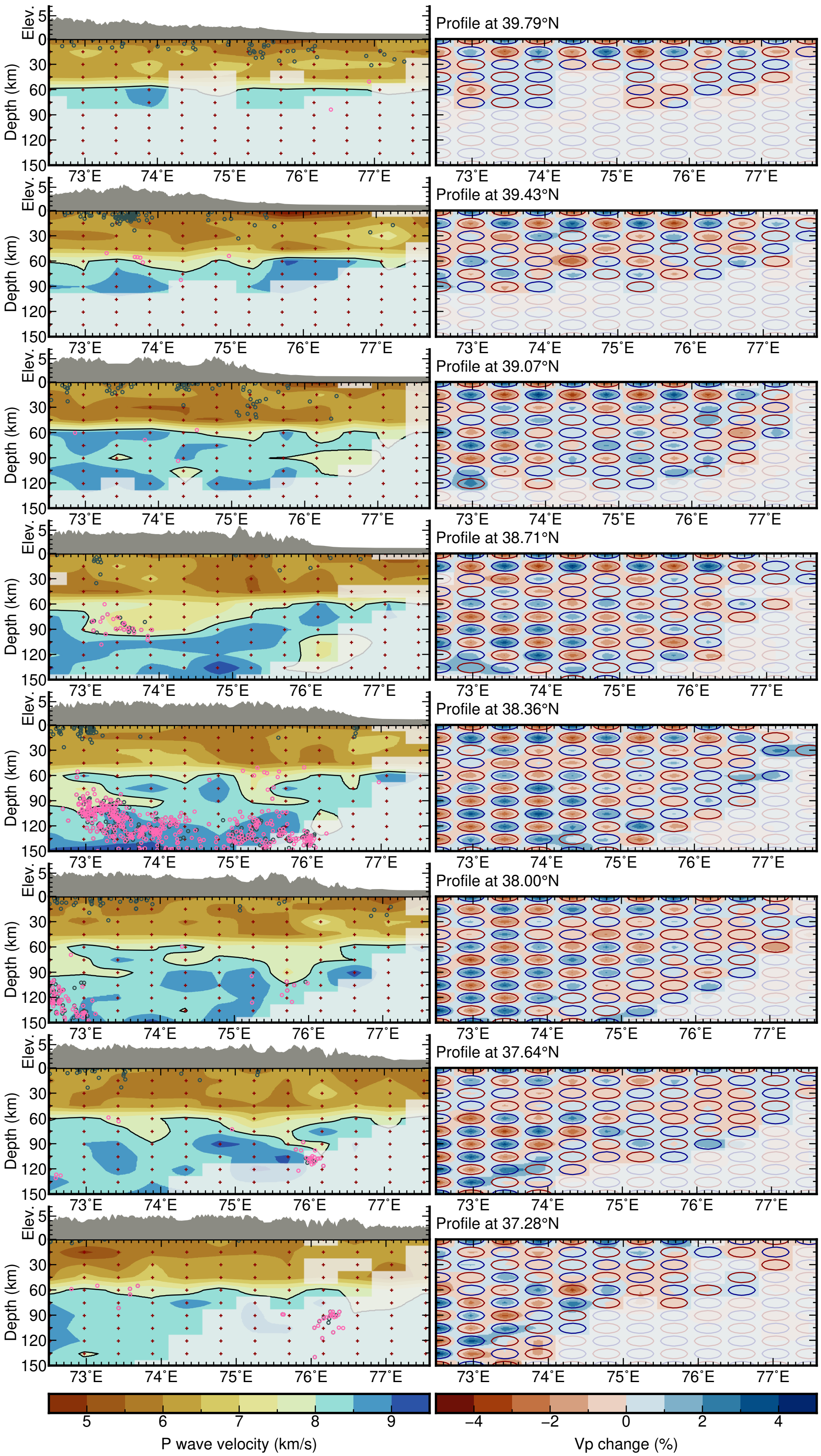

Figure S4. Same as Fig. S3, but with West-East-profiles.

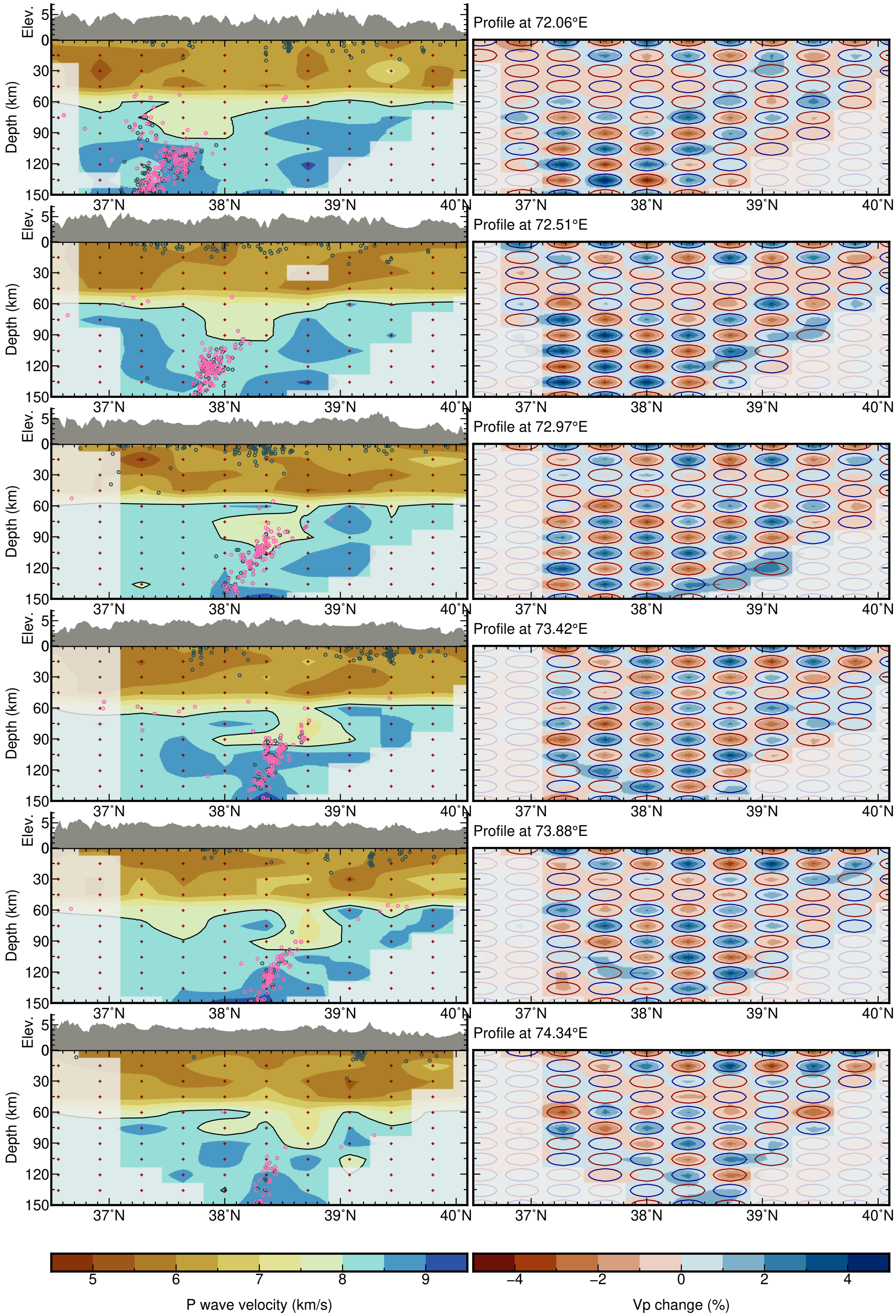

Figure S5. Same as Fig. S3, but with South-North-profiles.

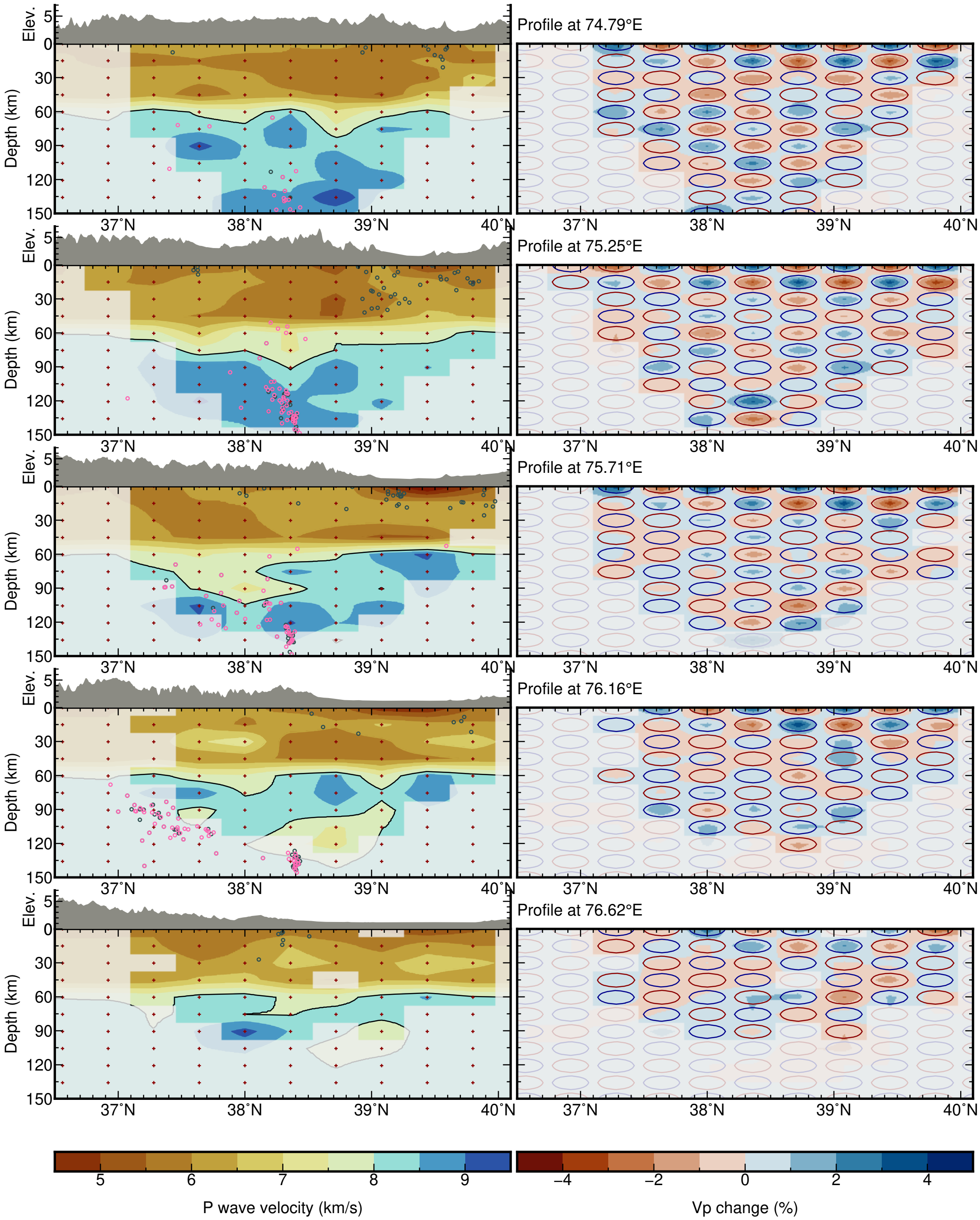

Figure S6. Fig. S5, continued